International Journal of Coal Science & Technology (2025) 12:54
https://doi.org/10.1007/s40789-025-00793-2

RESEARCH

Pore-scale evaluation of CO_2 miscible displacement in porous rocks induced by convection and diffusion: implications for CO_2 geo-sequestration

Xiangjie Qin[1] · Han Wang[1] · Jinsui Wu[2] · Gang Wang[3] · David A. Wood[4] · Jianchao Cai[1]

Received: 31 December 2024 / Revised: 18 March 2025 / Accepted: 15 April 2025

Abstract
CO_2 enhanced oil recovery plays an important role in carbon storage and utilization. However, the incomplete understanding of the underlying microscopic convection–diffusion mechanisms in complex pore structures has constrained the broader industrial application of CO_2 geo-sequestration. This work develops a pore-scale numerical model considering molecular convection–diffusion to investigate CO_2-oil miscible displacement in two- and three-dimensional porous structures of conglomerate rocks. The effects of CO_2 injection rates and pore structure properties on convection–diffusion are analyzed. By reconstructing the distribution of unexploited pores, the CO_2 sweep efficiency is quantitatively evaluated. Furthermore, a sequestration factor is proposed to evaluate the CO_2 storage capacity during miscible displacement. Convection significantly enhances the CO_2 mass fraction in fractures with high flow rates. Subsequently, CO_2 gradually diffuses into matrix pores without velocity distribution. Both convection and diffusion contribute to improving CO_2 displacement efficiency. Diffusion facilitates the dissolution of CO_2 into oil within small-diameter pores, and convection effectively mobilizes oil in large pore bodies. Developed and homogeneous pore structures enhance CO_2 displacement efficiency, whereas CO_2 flows along the main flow channels in heterogeneous pore structures, resulting in lower displacement efficiency. Diffusion plays a crucial role in CO_2 storage within porous media. At low injection rates, dissolved CO_2 is trapped in poorly connected and blind-end pores. The injection rate is negatively correlated with the sequestration factor.

Keywords Pore-scale simulation · CO_2 miscible displacement · Porous media · Convection and diffusion

1 Introduction

Reducing CO_2 emissions is essential for effectively controlling global warming and maintaining ecological balance (Iyer et al. 2022; Lee and Zhao 2023; Franck et al. 2024; Xu et al. 2024; Shang et al. 2024). Carbon Capture, Utilization, and Storage (CCUS) is a key strategy for reducing greenhouse gas emissions and enhancing the efficient development and utilization of fossil fuels (Edouard et al. 2023; Ge et al. 2023; Liu et al. 2023). As traditional oil and gas resources diminish, the development of low-permeability and tight oil reservoirs presents substantial potential (Du et al. 2023; Lu et al. 2024; Qin et al. 2024). CO_2 miscible flooding greatly enhances oil recovery and is a crucial aspect of CCUS (Liu et al. 2023; Zhang et al. 2023). The injected CO_2 dissolves in the crude oil, reducing density and viscosity and thereby enhancing the mobility of oil (Prasad et al. 2023; Cai et al. 2024b). Despite extensive efforts made in CO_2-enhanced oil recovery (CO_2-EOR) at the reservoir scale (Bachu. 2016; Alfarge et al. 2017), understanding the microscopic miscible flooding mechanisms remains challenging due to the fluid–fluid interactions associated with complex pore topology. This limits the in-depth application of CO_2-EOR. Therefore, it is essential to establish a pore-scale model to reveal the microscopic miscible flooding

✉ Jianchao Cai
caijc@cup.edu.cn

[1] State Key Laboratory of Petroleum Resources and Engineering, China University of Petroleum, Beijing 102249, China

[2] Department of Management Science and Engineering, Khalifa University, 127788, Abu Dhabi, United Arab Emirates

[3] College of Safety and Environmental Engineering, Shandong University of Science and Technology, Qingdao 266590, China

[4] DWA Energy Limited, Lincoln LN5 9JP, UK

Published online: 13 June 2025

mechanisms, providing theoretical guidance for optimizing CO_2 injection strategies and enhancing recovery.

Immiscible (Al-Bayati et al. 2018), near-miscible (Seyyedi and Sohrabi. 2020; Behnoud et al. 2023), and miscible flow (Yuan et al. 2023; Wan et al. 2024) are three modes of CO_2-EOR, which depend on the pressure and temperature conditions. In immiscible multiphase flows, the displacement is affected by contact angle and interfacial tension, which may result in oil being trapped within complex pore networks (Yang et al. 2025). Near-miscible flow occurs when CO_2 has low solubility in oil, allowing for mass transfer at the two-phase interface region (Alhosani et al. 2021). However, in miscible flows, the absence of interfacial tension between CO_2 and oil components allows CO_2 to displace oil trapped in complex pore networks through dissolution, thereby enhancing oil recovery (Ren et al. 2024). Actually, the temperature and pressure conditions of low-permeability and tight reservoirs are considerably higher than the minimum miscibility pressure (Wang et al. 2023b). Consequently, CO_2-oil miscible flow is a common scenario in engineering applications. The dispersion of CO_2 in porous media is a complex process affected by convection, diffusion, and pore structure properties. Experimental methods have been extensively employed to investigate the CO_2-oil miscible flow. Core flooding experiments provide globally sensitive parameters, such as injection pressure and flow rate, to predict internal flow characteristics (Chen et al. 2022a). Additionally, by integrating with nuclear magnetic resonance (NMR), residual oil distribution characteristics are further analyzed, allowing for the assessment of CO_2 sweep efficiency (Wei et al. 2020; Li et al. 2021). Core-based experiments provide insights primarily into global flow behaviors and cannot examine the internal microscopic convection–diffusion mechanisms. Microfluidic experiments, combined with microscopic imaging systems, facilitate visual and quantitative description of miscible and immiscible flows (Ho et al. 2021; Zou et al. 2024). It directly observes the interaction mechanisms between CO_2 and oil at the pore-scale (Hao et al. 2022). However, the fabrication process for high-precision microfluidic chips with complex pore topology is intricate, and there are significant differences compared to the actual three-dimensional (3D) pore structures of reservoirs.

Numerical simulation has become a commonly used technique for investigating complex fluid flow behaviors within micro- and nanoscale pores (Ramstad et al. 2019; Wang et al. 2024a; Yin et al. 2024). Molecular dynamics (MD) simulations provide a detailed understanding of the mechanisms underlying CO_2-oil miscible flow at the molecular level, accurately describing molecular collisions, adsorption, and diffusion processes (Cai et al. 2024a; Wu et al. 2024). However, MD simulations require substantial computational resources for complex pore systems and prolonged simulation durations. It is commonly employed to investigate the flow characteristics within single nanopores. Pore-scale simulations considering adsorption, convection, and diffusion effects establish a bridge between macroscopic flows and the microscopic flow mechanisms described by MD simulations (Chen et al. 2022b; Yang et al. 2023). It accurately replicates the CO_2-oil miscible flow within complex pore topology and produces representative results, offering valuable insights to inform the development process (Chowdhury et al. 2022; Wang et al. 2023a). Numerous studies have investigated CO_2-oil miscible flow through pore-scale simulations. Wang et al. (2022) modified the pore-scale simulation parameters based on MD simulation results, developing a multiple relaxation time lattice Boltzmann method that accounts for the competitive adsorption and diffusion behaviors in CO_2-oil miscible system. For the CO_2-oil miscible displacement process, Zhu et al. (2024) analyzed the convection–diffusion effects of CO_2-oil in two-dimensional (2D) porous media using pore-scale simulations. They concluded that molecular convection and diffusion influence the displacement patterns, while fracture inclination and connectivity affect breakthrough events. Currently, the mechanisms by which convection–diffusion affects CO_2-oil miscible flow remain unclear in reservoirs due to the complex pore topology. Randomly generated geometric models fail to capture the actual pore structure properties of porous rocks, making it difficult to accurately assess CO_2 sweep efficiency. Additionally, a significant amount of research has focused on investigating CO_2-oil miscible displacement process for enhanced recovery, while the assessment of CO_2 sequestration capacity has received little attention.

Therefore, a comprehensive analysis of the molecular convection–diffusion effects of CO_2-oil miscible flow is performed within 2D and 3D porous media, integrating advanced image processing techniques to quantitatively assess CO_2 sweep efficiency and sequestration capacity. First, 2D and 3D porous structures that accurately reflect the actual pore topology are constructed using micro-CT images of conglomerate rocks. Then, a pore-scale numerical model considering molecular convection–diffusion is developed to simulate CO_2-oil miscible displacement at different injection rates within porous structures. Convection–diffusion effects are identified in complex pore-fracture networks. Finally, the distribution characteristics of unexploited pores are reconstructed, and a sequestration factor is proposed to evaluate the CO_2 storage capacity under different injection rates.

2 Image reconstruction of complex pore structures

2.1 Micro-CT experiments

Two conglomerate samples, S1 and S2, are selected from the Mahu Depression for micro-CT scanning experiments. The samples exhibit well-developed intergranular pores and microfractures, with strong pore connectivity. The porosities of S1 and S2 are 12.9% and 11.2%, respectively, while their permeability values are 0.87 and 0.30 mD. The porosity and permeability of the selected samples align with the distribution range of conglomerate reservoirs in the Mahu Depression (Tang et al. 2025), confirming their representativeness. In addition, the considerable difference in permeability between the two samples provides an opportunity to analyze the impact of pore structure properties on fluid flow. Cylindrical samples with a diameter of 5 mm are cut from standard cores using the wire-cutting method for CT scanning. The scanning equipment is manufactured by Sanying Precision with a resolution of 1.86 μm. Figure 1 illustrates the scanning results of the conglomerate rocks, revealing a significant presence of intergranular pores and microfracture structures. S1 exhibits well-developed intergranular pores and microfractures, demonstrating strong connectivity (Fig. 1a). In contrast, S2 primarily features microfractures, with particles arranged closely together (Fig. 1b). The pore structure properties obtained from the CT scanning experiments correspond to the porosity and permeability characteristics of the samples.

2.2 Reconstruction of 2D and 3D porous media

Due to the strong heterogeneity of conglomerate rocks, the pore structures of different slices exhibit significant variations. To construct 2D porous media, slices with porosity closely matching that of the sample are selected. Furthermore, an interpolation algorithm is implemented to enhance the image resolution to 0.93 μm, facilitating the identification of matrix pores. Images are cropped for threshold segmentation to extract the complex pore structures. The interactive threshold segmentation method based on grayscale values is combined with the top-hat segmentation method to extract large pore bodies and microfractures respectively. The segmentation results are fused by arithmetic addition. Since pore structures are isolated in a 2D perspective, they cannot form connected flow channels. However, these pores may be interconnected to form complex pore networks in the 3D perspective. To construct 2D connected pore networks, distance transformation and watershed algorithms are introduced to separate the rock matrix and connect isolated pores (Fig. 2a). Firstly, the matrix area is marked through image segmentation, and the shortest distance from the marked area to the boundary is counted to generate a distance map. Then, the watershed algorithm based on morphology theory is applied to generate segmentation lines to separate the rock matrix and connect isolated pores. Finally, 2D porous structures of conglomerate rocks are established for CO_2-oil miscible flow based on CT images. In 2D porous media, the pore diameter follows a unimodal distribution (Fig. 2b). Well-developed fracture structures exist in S1, and the pore diameters are broadly distributed within the 6 to 12 μm. In contrast, the pore diameters are concentrated in the range of 6 to 10 μm in S2.

Since the 3D simulation is computationally expensive, a subdomain with a size of 186^3 μm^3 is extracted for model reconstruction. Representative elementary volume analysis demonstrates that when the model size surpasses this threshold, the porosity gradually stabilizes. The grayscale images are filtered and segmented to generate a 3D structure (Fig. 2c). To quantitatively describe the complex

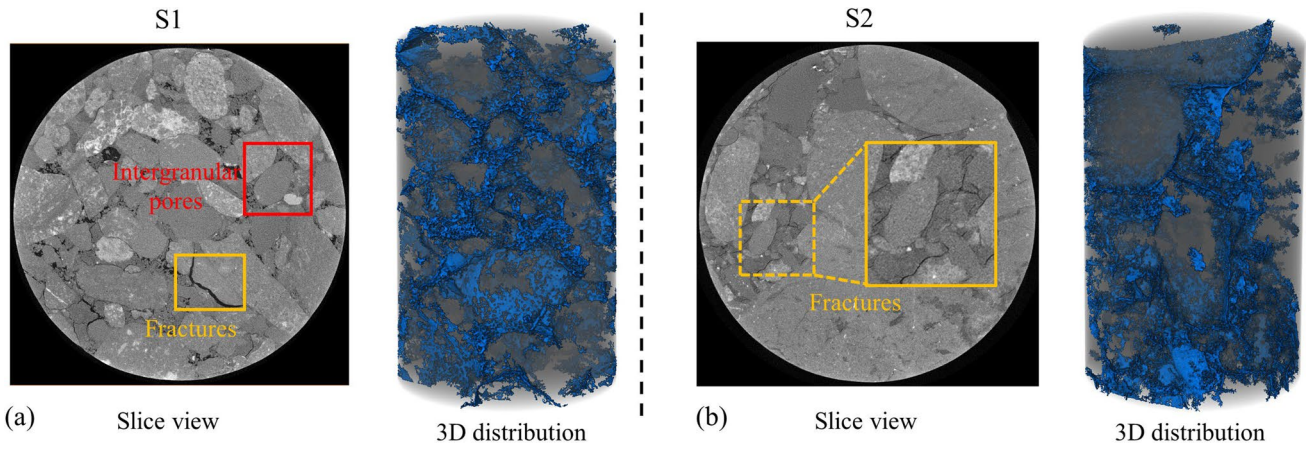

Fig. 1 CT scanning results of conglomerate rocks. **a** S1; **b** S2

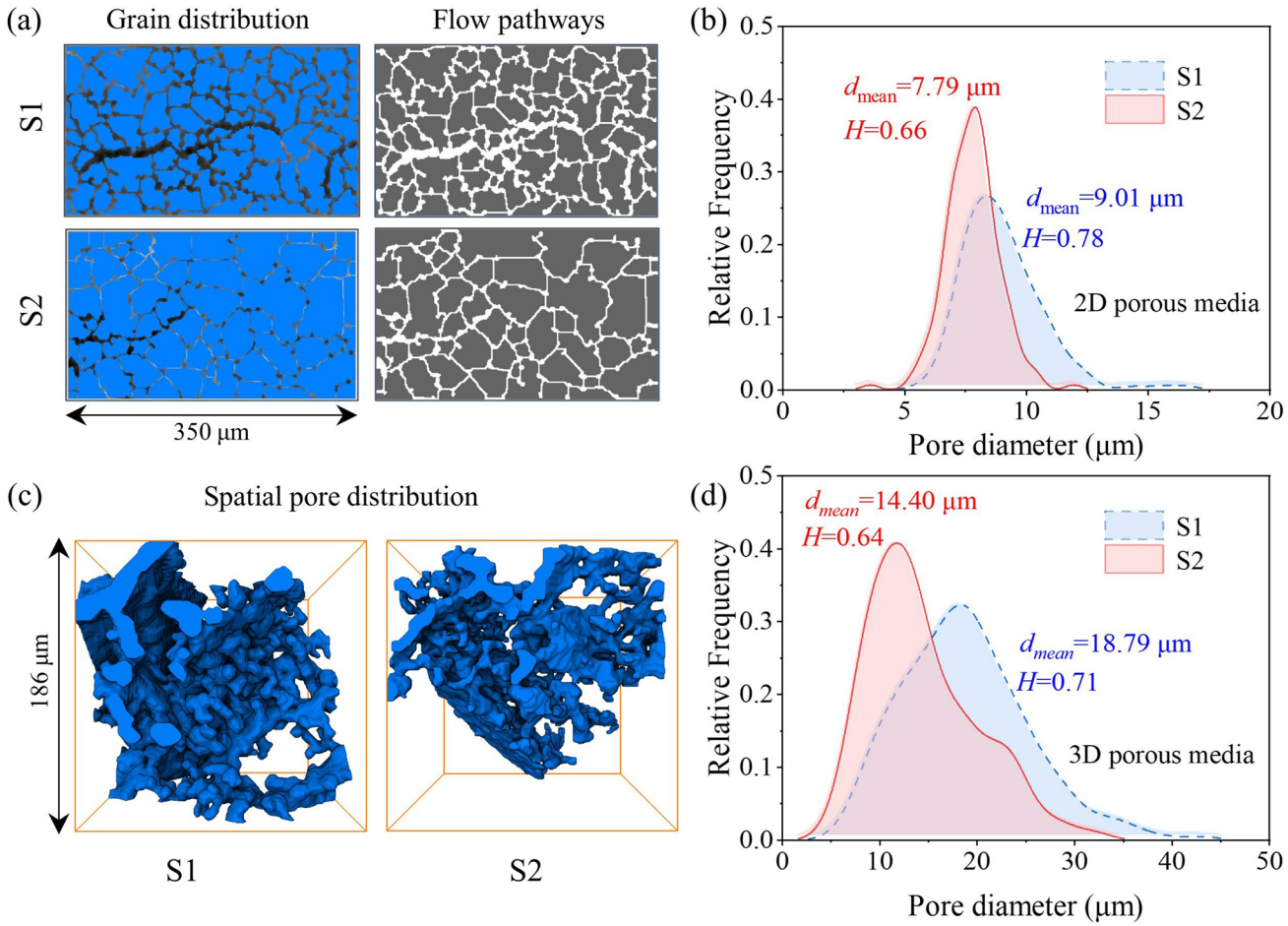

Fig. 2 Pore structure properties of conglomerate rocks. **a** Generation of 2D porous media; **b** Pore size distribution of 2D porous media; **c** 3D pore structures; **d** Pore size distribution of 3D porous media

pore structures, the watershed algorithm is applied to identify pore-throat structures and generate the pore network model. Well-developed fracture structures exist in 3D porous media and the fractures are connected with matrix pores, forming complex pore networks. The pore diameters of S1 are mainly distributed in the range of 10 to 25 μm. The pore sizes of S2 are relatively small and the distribution is concentrated. The pores within the diameter of 10 to 15 μm account for 41% of the total (Fig. 2d).

In addition, pore heterogeneity significantly influences the flow process. Entropy is introduced to describe the heterogeneity of the pore size distribution (Zhang et al. 2022):

$$H = -\sum_{k} P(k) \log P(k) \tag{1}$$

where k represents the specific pore size distribution range, and $P(k)$ is the pore size distribution frequency within the range k.

When the pore sizes in the model are uniform, the value of entropy is 0, indicating a homogeneous pore size distribution. The larger the entropy, the stronger the heterogeneity of pore structures. Based on this, the heterogeneity for 2D porous media of S1 and S2 is calculated to be 0.66 and 0.78, respectively, while the heterogeneity for 3D porous media of S1 and S2 is calculated to be 0.64 and 0.71, respectively.

3 Pore-scale model for CO_2-oil miscible flow

3.1 Numerical model

The numerical model assumes that CO_2-oil is mixed at the molecular scale and they share the velocity and pressure fields, with no interfacial tension between CO_2 and oil components. Since the impact of adsorption on fluid flow is negligible in microscale porous media, adsorption effects are not considered in the CO_2-oil flow process. A fluid mixture containing oil and CO_2 components is

defined to obtain the global velocity and pressure fields. During the miscible displacement process, bulk oil, bulk CO_2, and dissolved CO_2-oil may coexist in the fluid mixture. The mass transfer between components in the fluid mixture is controlled by molecular convection and diffusion, and the diffusion velocity follows Fick's law.

The transport for multi-component fluids satisfies the conservation of momentum (i.e., the NS equation):

$$\overline{\rho}\left(\frac{\partial \boldsymbol{u}}{\partial t}+\nabla\cdot\boldsymbol{u}\cdot\boldsymbol{u}\right)=-\nabla p+\nabla\cdot\tau+f \tag{2}$$

where, $\overline{\rho}$ is the density of the fluid mixture, $\boldsymbol{u}$ is the average velocity field, p is the pressure, τ is the stress tensor, and f is the body force.

Additional equations are introduced to solve the transport of CO_2 and oil components in a fluid mixture. The mass conservation equation for each component is:

$$\frac{\partial \rho_i}{\partial t}+\frac{\partial\left(\rho_i \boldsymbol{u}\right)}{\partial x}=-\frac{\partial M}{\partial x} \tag{3}$$

where ρ_i is the mass-average density of component i in the mixture, and M is the relative mass flux. The relative mass flux term reflects the differing motions of each individual component. The concentration gradient mainly affects the mass transfer between components. A diffusion-like term is given for the diffusion effects:

$$M=-\frac{\alpha}{\overline{\rho}}\frac{\partial \rho_i}{\partial x} \tag{4}$$

where, α is the molecular diffusion coefficient.

Assuming the system contains components i and j, during the miscible flow process, the increase in the mass of component i is equal to the decrease in the mass of component j. Therefore, summing all the terms in the expanded form of Eq. (3) across all components yields the standard continuity equation:

$$\frac{\partial \overline{\rho}}{\partial t}+\frac{\partial\left(\overline{\rho}\boldsymbol{u}\right)}{\partial x}=0 \tag{5}$$

The mass fraction of component i is defined as the ratio of the mass of component i to the total mass of the fluid mixture. The mass fraction is described by transforming the fluid densities:

$$\varphi_i=\frac{\rho_i}{\overline{\rho}} \tag{6}$$

where φ_i is the mass fraction of component i.

Substituting Eq. (4) and Eq. (6) into Eq. (3) to obtain the general convection–diffusion equation (Teng et al. 2021):

$$\frac{\partial(\overline{\rho}\varphi_i)}{\partial t}+\frac{\partial(\overline{\rho}\boldsymbol{u}\varphi_i)}{\partial x}=\frac{\partial}{\partial x}\left(\alpha\frac{\partial\varphi_i}{\partial x}\right) \tag{7}$$

The mass fraction of CO_2 is obtained by solving the mass fraction equations of the CO_2 component. The sum of the mass fractions of CO_2 and oil components must be 1. Therefore, the mass fraction of the oil component defined as the constraint component is obtained by the constraint equation:

$$\sum_{i=A,B}^{N}\varphi_i=1 \tag{8}$$

The physical properties of the fluid mixture are directly calculated from the properties of the CO_2 and oil components and their proportions in the fluid mixture. Partial volume (V_{si}) is defined as the equivalent volume of component i under standard conditions. The sum of the partial volumes of all components equals the volume V of the fluid mixture:

$$1=\sum_{i=A,B}^{N}\frac{V_{si}}{V}=\sum_{i=A,B}^{N}\frac{M_i/\rho_{si}}{M_i/\rho_i}=\sum_{i=A,B}^{N}\frac{\rho_i}{\rho_{si}} \tag{9}$$

where ρ_{si} is the actual thermodynamic density of component i, and M_i is the mass of component i.

Combined with Eq. (6), it can be transformed into:

$$1=\sum_{i=A,B}^{N}\frac{\overline{\rho}\varphi_i}{\rho_{si}} \tag{10}$$

Therefore, the density of fluid mixture can be obtained by the mass fraction and thermodynamic density of each component:

$$\frac{1}{\overline{\rho}}=\sum_{i=A,B}^{N}\frac{\varphi_i}{\rho_{si}} \tag{11}$$

In addition, arbitrary constitutive fluid properties such as viscosity can be obtained by:

$$\overline{\chi}=\sum_{i=A,B}^{N}\varphi_i\chi_{si} \tag{12}$$

where $\overline{\chi}$ is the property of the fluid mixture, and χ_{si} is the actual fluid property of component i.

The CO_2 density and viscosity parameters are obtained from the NIST standard reference database at 60 ℃ and 15 MPa. Based on this, the density and viscosity ratios of oil-CO_2 are adjusted to 2 and 20, highlighting the simulation effects. Additionally, referring to the studies by Zhu et al. (2024) and Li et al. (2016), the diffusion coefficient is estimated to be 2×10^{-9} m^2/s. During the miscible flow

of supercritical CO_2 and oil, the density and viscosity of fluid mixture decrease with increasing CO_2 mass fraction. Substituting the density parameters into Eq. (11) yields the expression for the density of fluid mixture as a function of CO_2 mass fraction (Fig. 3a). The relationship between the density and CO_2 mass fraction shows a power function. As the CO_2 mass fraction increases, the density decrease rate decreases gradually. Similarly, by combining Eq. (12), the expression for the viscosity of fluid mixture as a function of CO_2 mass fraction is obtained (Fig. 3b). The viscosity is linearly negatively correlated with the CO_2 mass fraction.

3.2 Validation of CO_2-oil miscible flow

The CO_2-oil miscible flow numerical model is validated by comparing the simulation results with the microfluidic experiments conducted by Li et al. (2023). The microfluidic model is initially saturated with oil, and CO_2 is injected from the left side at a velocity of 0.004 m/s. CO_2 dissolves the oil in the vertical channel under diffusion, increasing the sweep area. The distribution of CO_2 mole fraction is consistent with the results of microfluidic experiments during the displacement (Fig. 4a). As the displacement proceeds, CO_2 dissolves the oil in the vertical channel, and the oil mole fraction gradually decreases. Along the direction of CO_2 diffusion, the molar fraction of oil increases, and the

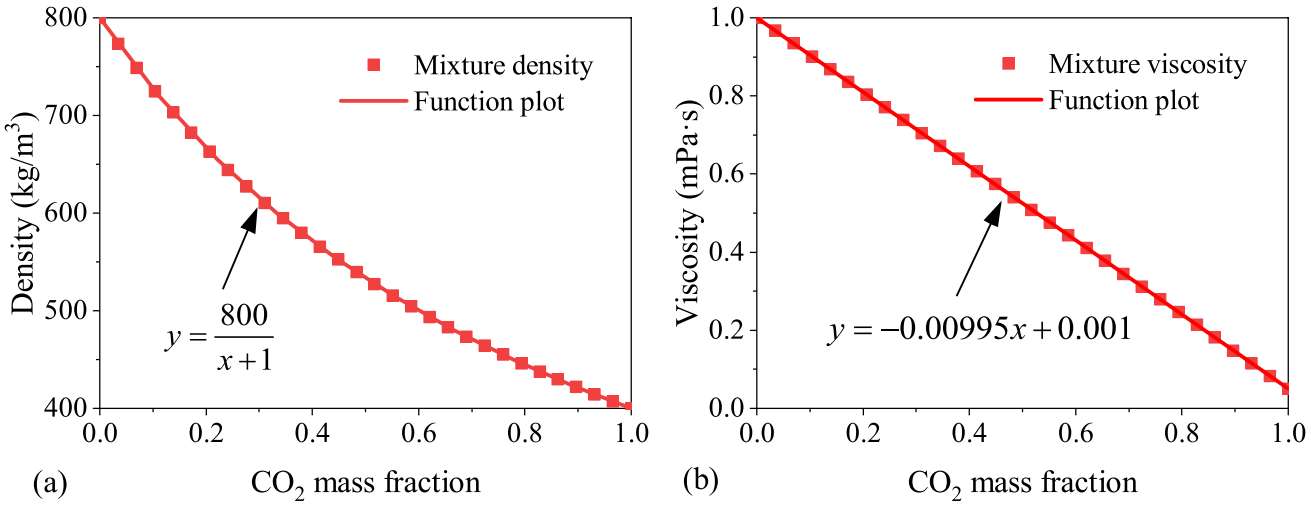

Fig. 3 Variation of miscible fluid properties. **a** Density; **b** Viscosity of fluid mixture are functions of CO_2 mass fraction

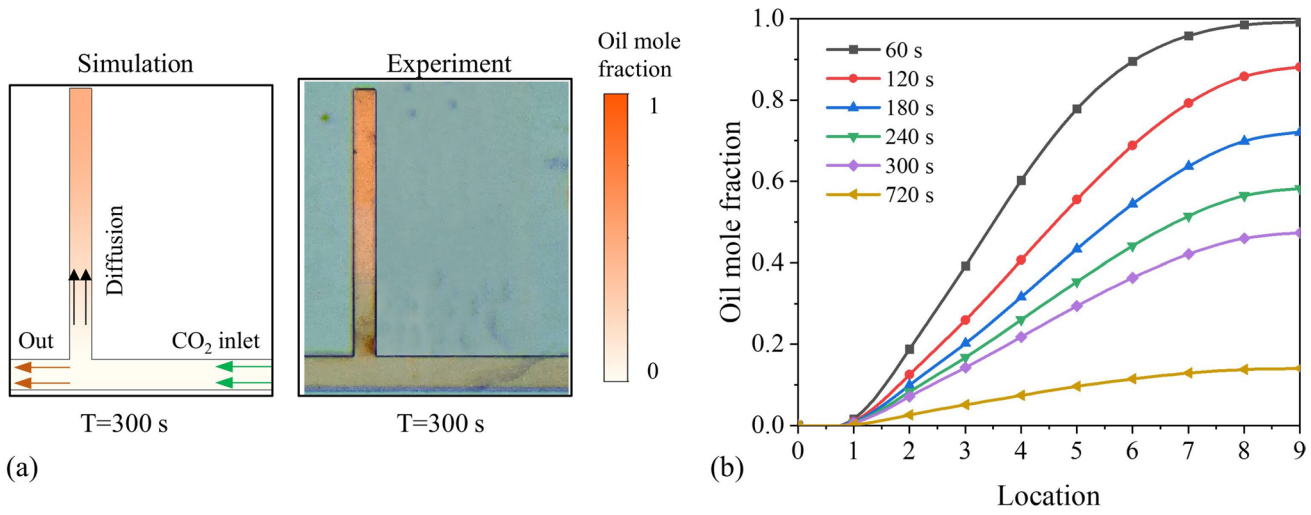

Fig. 4 Experimental verification of the CO_2-oil miscible flow numerical model. **a** Oil mole fraction distribution in microfluidics obtained from simulation and experiment; **b** Variation of oil mole fraction along the diffusion direction

increase rate of oil mole fraction gradually decreases in the vertical channel (Fig. 4b). The distribution of oil mole fraction corresponds to the analysis results of Li et al. (2023). Therefore, the numerical model is reasonable for the prediction of CO_2-oil miscible flow.

3.3 2D and 3D simulation schemes

To complete the numerical discretization calculation, the complex pore topology is divided into a series of hexahedral meshes, with the element size of 1 μm. The meshing of the complex pore system is completed in snappyHexMesh. The hexahedral background mesh is generated through the blockMesh module to cover the surface model of the pore topology, retaining the grids in the surface model to complete the meshing. Flow processes are solved in x, y, and z directions for 3D porous media. Symmetric boundary conditions are introduced for 2D porous media, in which the flow processes are solved in the x and y directions. The solution is completed in the CFX-solver manager using the second-order backward Euler algorithm to deal with transient flow processes with a solution accuracy of 10^{-6}.

CO_2-oil miscible displacement processes are conducted in pore systems of saturated oil at different CO_2 injection rates (Table 1). The appropriate CO_2 injection volume is crucial for subsequent analysis. A low CO_2 injection volume prevents CO_2 from breaking through at the outlet, while continuous CO_2 injection results in CO_2 dissolving into the oil in poorly connected networks and blind-end pores, ultimately causing the recovery efficiency to approach unity. Therefore, both excessively low and high CO_2 injection volumes are unsuitable for analyzing the influencing factors of miscible displacement. In the simulation, 1.5 PV of CO_2 is injected to analyze the miscible displacement process under different conditions. Convection and diffusion jointly affect CO_2 dissolution. The Peclet number is introduced to describe the strength of convection and diffusion effects. A large Peclet number indicates a high flow rate, where convection dominates the concentration changes, while a small Peclet number suggests that diffusion is the primary influence on concentration changes. The Peclet number can be calculated as the ratio of injection velocity to the diffusion coefficient (Wang et al. 2024b):

$$\mathrm{Pe} = \frac{u_0 \cdot h_0}{\alpha} \tag{13}$$

where u_0 is the initial flow velocity and h_0 is the fluid height. For porous media flows, h_0 is determined by porosity (ϕ) and permeability (K):

$$h_0 = \sqrt{\frac{12K}{\phi}} \tag{14}$$

Table 1 Simulation schemes

Structures	CO_2 injection rate (m/s)	Injection volume (PV)	Peclet number
S1 2D porous media	0.001	1.5	0.968
	0.005	1.5	4.84
	0.01	1.5	9.68
	0.05	1.5	48.4
S2 2D porous media	0.001	1.5	0.826
	0.005	1.5	4.13
	0.01	1.5	8.26
	0.05	1.5	41.3
S1 3D porous media	0.0005	1.5	1.06
	0.001	1.5	2.12
	0.005	1.5	10.6
	0.01	1.5	21.2
	0.05	1.5	106
S2 3D porous media	0.0005	1.5	0.61
	0.001	1.5	1.22
	0.005	1.5	6.1
	0.01	1.5	12.2
	0.05	1.5	61

4 Results and discussion

4.1 Convection and diffusion effects in the miscible displacement process

The CO_2-oil miscible displacement processes in 2D and 3D porous media are obtained respectively. Figure 5 illustrates the displacement process of model S1. There is no distinct interface between CO_2 and oil components, indicating that CO_2 is dissolved in the oil during the displacement. Without the effect of capillary force, the injected CO_2 prefers to flow along the pore center and quickly breaks through the outlet along the dominant channels. CO_2 channeling is significant in fracture structures and breaks through the outlet earlier. Subsequently, CO_2 gradually occupies the pore spaces under convection and diffusion effects. After the breakthrough, due to the concentration difference of CO_2 in fractures and matrix pores, CO_2 gradually dissolves into the matrix pores and expands the swept area.

Convection and diffusion are the important mechanisms of mass transfer in miscible flows. The convection and diffusion phenomena are explained based on the 2D simulation results. The mass transfer between CO_2-oil components controlled by convection is caused by the pressure gradient. Due to the constant injection rate, fluid pressure decreases along the flow direction. Therefore, the variation of CO_2 mass fraction caused by the convection is dominant along

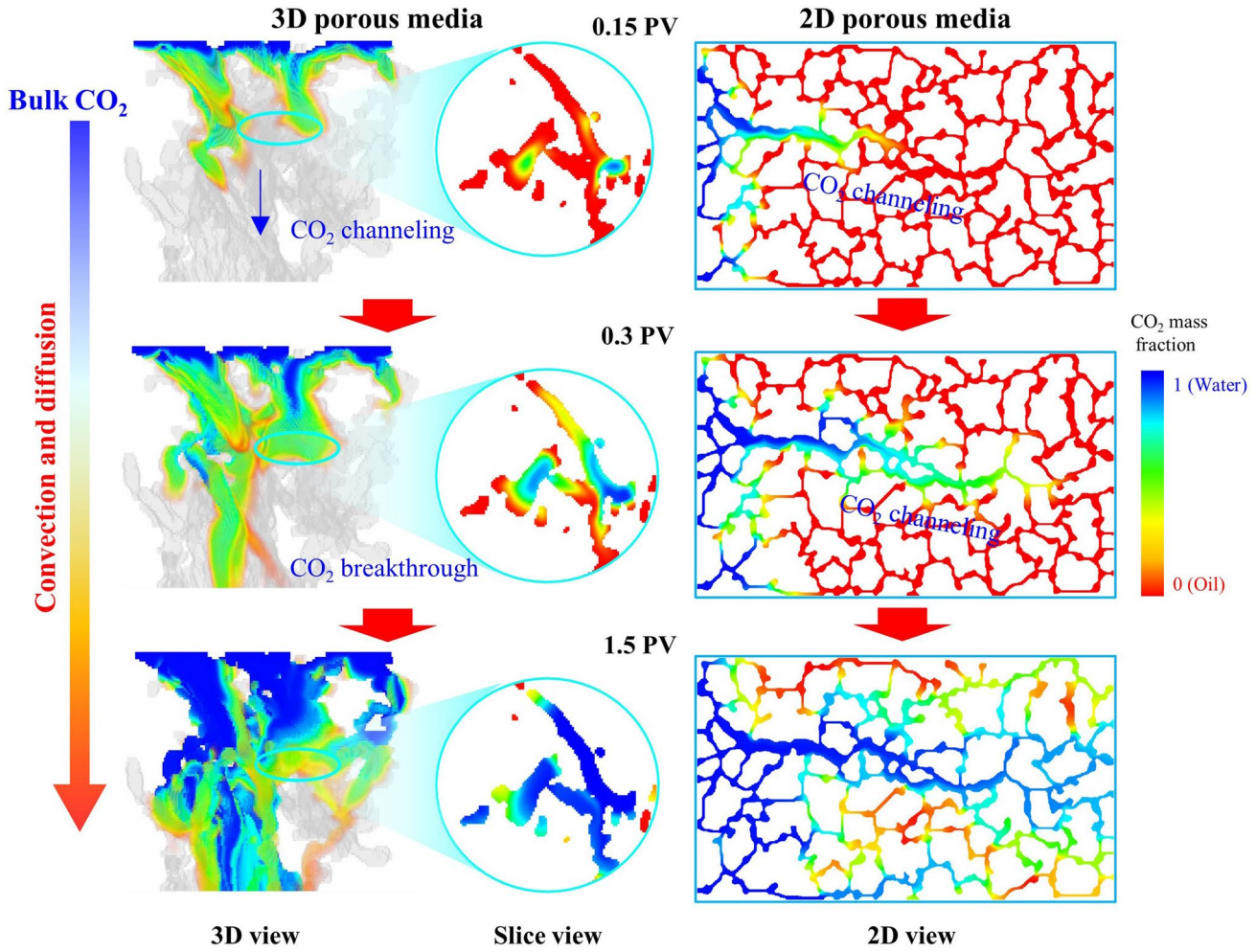

Fig. 5 Variation of CO_2 mass fraction in 2D and 3D porous media during miscible displacement

the flow direction. In addition, due to CO_2 channeling, convection dominates the miscible displacement before CO_2 breakthrough. Diffusion is caused by concentration differences between components. After the breakthrough, the bulk CO_2 in fractures diffuses into the oil-saturated matrix pores in different directions (Zhu et al. 2024). The distribution of velocity streamlines in the pore system reveals a concentration in the fracture structures (Fig. 6a), where the velocity values are significantly higher than those in the matrix pores (Fig. 6b). Affected by the fracture inclination angle, only a few velocity streamlines are distributed at the bottom of the model. In the upper region and certain areas at the bottom of the porous media, there are no velocity streamlines, indicating that the flow velocity is minimal in the matrix pores (Fig. 6a), with diffusion dominating the mass transfer between CO_2 and oil components (Fig. 6c). The changes in CO_2 mass fraction in fractures and matrix pores are extracted. Under the convection effect, the mass fraction of CO_2 in fractures increases rapidly after injecting a small amount of CO_2. In contrast, due to the diffusion effect, the mass fraction of CO_2 in the matrix pores increases slowly with increasing CO_2 injection amount (Fig. 6d). Furthermore, with continued CO_2 injection, the concentration difference of CO_2 in fractures and matrix pores decreases, and the increase rate of CO_2 mass fraction gradually slows down.

4.2 Fluid flow characteristics

The mass fraction and volume fraction of CO_2 increase during the displacement process (Fig. 7a). Due to the constant injection rate, the volume fraction of CO_2 increases linearly with increasing injection volume before the breakthrough event. The mass fraction is less than the volume fraction during the displacement because the injected CO_2 reduces the density of the fluid mixture. CO_2 breaks through the outlet earlier in 3D pore systems, resulting in a lower oil recovery compared to the simulation results

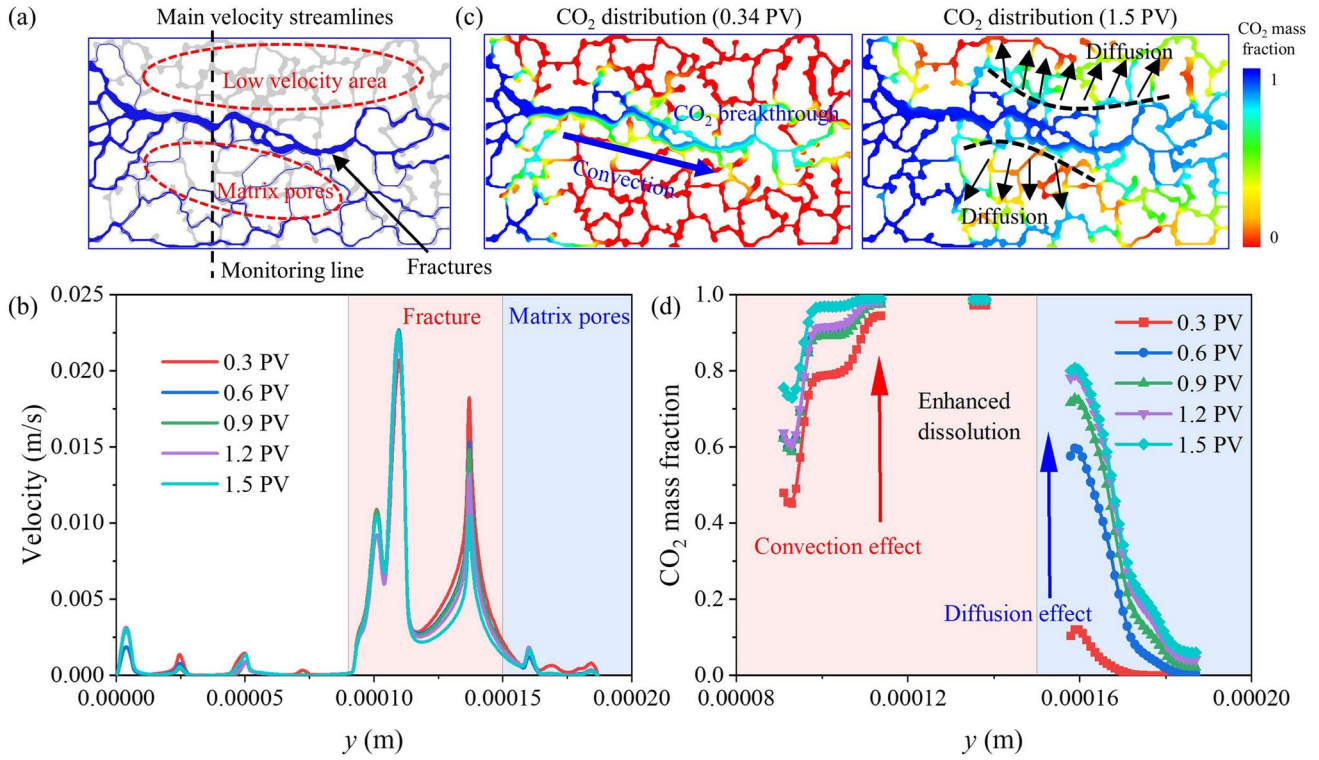

Fig. 6 Convection–diffusion in fractures and matrix pores. **a** Velocity streamlines distribution in porous media; **b** Velocity values in fractures and matrix pores; **c** CO_2 mass fraction distribution in porous media; **d** CO_2 mass fraction changes in fractures and matrix pores

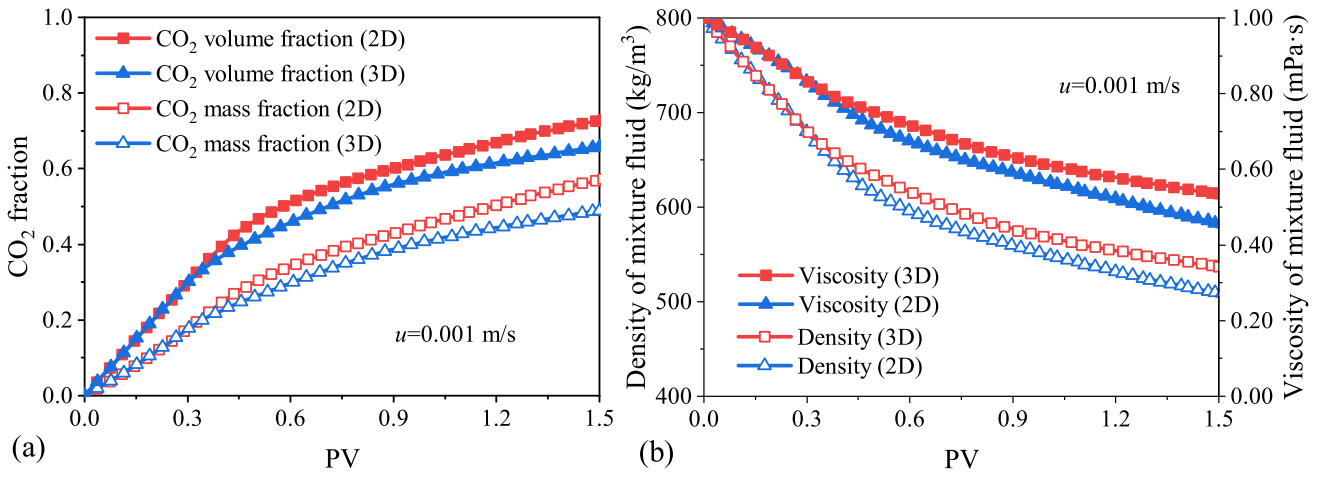

Fig. 7 Variation of **a** CO_2 mass fraction and volume fraction, and **b** The density and viscosity of the fluid mixture during the displacement process

of 2D porous systems. The increasing rates of CO_2 mass fraction and volume fraction gradually decrease after the CO_2 breakthrough. Besides, the increasing rate remains high after injecting 1.5 PV of CO_2 due to the continuous dissolution of CO_2 into the oil under the diffusion effect. With the continuous injection of CO_2, the oil will be completely displaced in complex pore systems. The density and viscosity of the fluid mixture are functions of the CO_2 mass fraction. As the volume of CO_2 injected increases, the density and viscosity of fluid mixture gradually decrease (Fig. 7b). After injecting 1.5 PV of CO_2, the fluid viscosity in the 3D and 2D pore systems decreased by 46.5% and 54.3%, respectively, while the fluid density decreased by 32.9% and 36.4%.

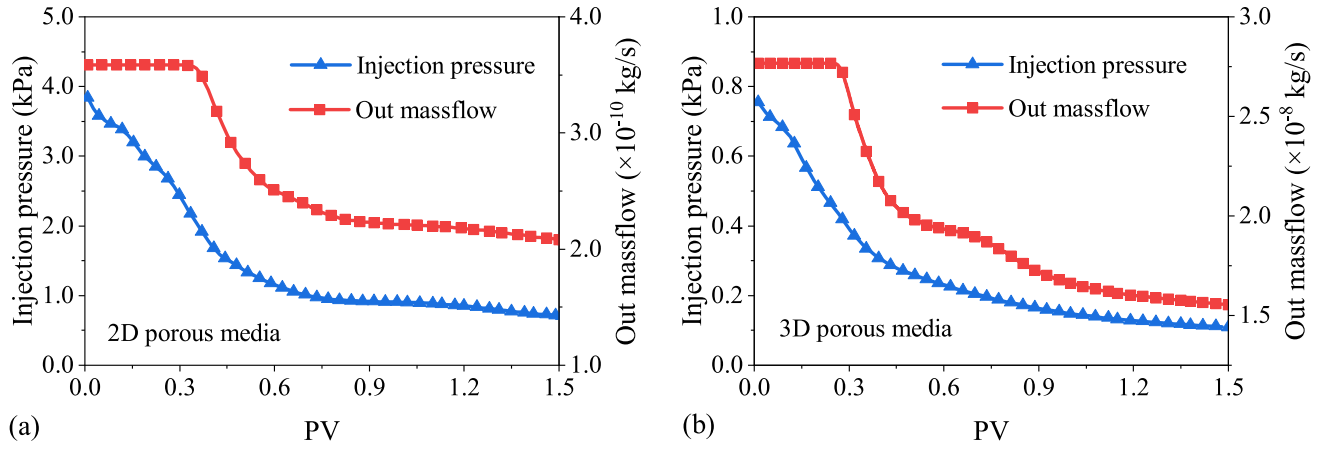

Fig. 8 Variation of injection pressure and outlet mass flow in **a** 2D and **b** 3D porous media

The injection pressure decreases with increasing CO_2 injection volume in 2D (Fig. 8a) and 3D (Fig. 8b) porous media, as the injected CO_2 reduces the density and viscosity of the fluid mixture. Before CO_2 breakthrough, the outlet mass flow remains constant, with a significant amount of oil flowing out of the pore system. The presence of bulk and dissolved CO_2 in the pore system results in a significant reduction in fluid pressure. After the breakthrough, the outlet mass flow decreases rapidly, indicating that a large amount of bulk CO_2 is exiting the pore system due to strong convection effects. Subsequently, the pressure and outlet mass flow decline gradually, indicating that CO_2 continues to dissolve in the oil through the diffusion effect.

4.3 Effect of injection velocity and pore structure properties

The injection velocity affects the convection and diffusion behaviors within complex pore structures, with its impact appearing to differ between 2 and 3D perspectives (Fig. 9). In 2D porous media, high injection velocity causes CO_2 to break through prematurely at the outlet (Li et al. 2023). Conversely, at low injection rates, the strong diffusion effect delays breakthrough and expands the CO_2 sweep range. Thus, injection velocity is negatively correlated with CO_2 mass fraction and oil recovery (Figs. 9a, b). In 3D porous media, the convection–diffusion effects differ significantly from those in 2D porous media. Velocity variations have a slight influence on oil recovery within the range of 0.0005 to 0.01 m/s, but recovery improves significantly when the injection velocity increases to 0.05 m/s (Fig. 9c). As the injection rate increases, the oil recovery displays a trend of first decreasing and then increasing (Fig. 9d). This suggests that strong convection effects in 3D porous media may increase displacement channels and enhance recovery (Ren et al. 2024).

The variations of outlet mass flow under different injection velocities are further analyzed (Fig. 10). To facilitate comparison, the outlet mass flow rates are normalized. The attenuation characteristics of the outlet mass flow provide valuable insights into CO_2 sequestration and oil recovery. In a 3D porous medium, the volume of injected fluid corresponding to the breakthrough event is nearly constant at different CO_2 injection velocities (Fig. 10a, b). However, the outlet mass flow decays slowly at high injection velocities, indicating a high concentration of the oil component in the fluid mixture. Additionally, diffusion effects may delay the CO_2 breakthrough event and the decline in outlet mass flow at low injection velocities. Therefore, the diffusion effects caused by low flow velocity and the convection effects caused by high flow velocity can improve the oil recovery in 3D porous media. As a result, the oil recovery decreases first and then increases with increasing injection rate, with the critical velocity 0f 0.005 m/s. In 2D porous media, high injection rates cause CO_2 to break through the outlet prematurely, and the outlet mass flow decays rapidly, corresponding to poor displacement efficiency (Fig. 10c, d). Due to differences in pore structure properties, the relationship between injection rate and recovery varies between 2 and 3D porous media. Therefore, within the same pore topology, the Peclet number is negatively correlated with oil recovery in 2D porous media, while in 3D porous media, the relationship shows an initial decrease followed by an increase in oil recovery.

The distribution of CO_2 mass fraction in the complex pore structures is extracted to analyze the displacement behavior at different injection rates (Fig. 11). The diffusion effect becomes pronounced at low injection rates due to the extended diffusion time. In this scenario, CO_2 dissolves into the oil along the vertical direction, enhancing the sweep efficiency (Fig. 11a). However, limited by the diffusion rate, it takes a long time to achieve satisfactory displacement

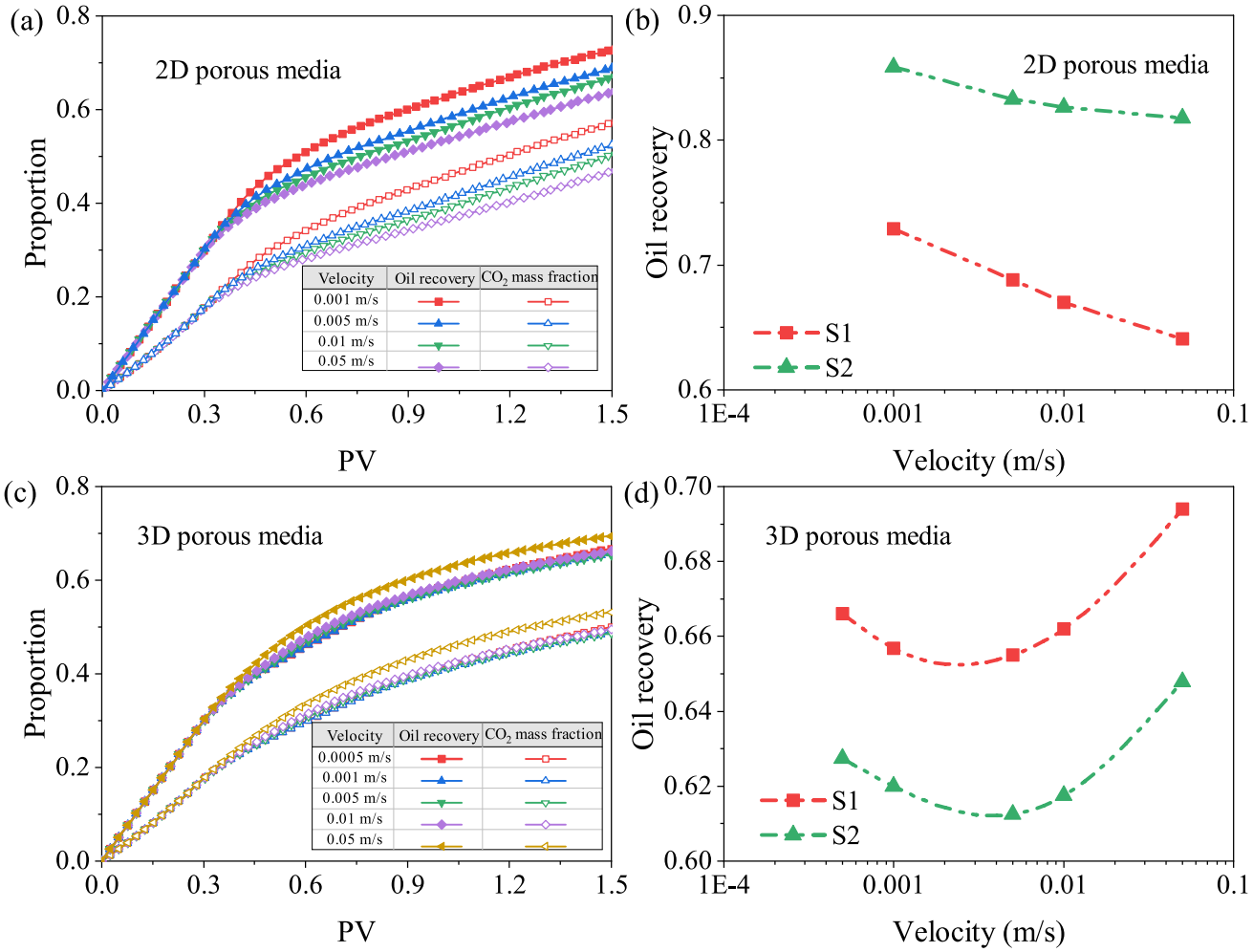

Fig. 9 Effect of injection rates on miscible displacement. In 2D porous media, **a** Changes in CO_2 mass fraction and oil recovery and **b** Oil recovery as a function of injection rate. In 3D porous media and **c** Changes in CO_2 mass fraction and oil recovery and **d** Oil recovery as a function of injection rate

results. High injection rates indicate strong convective effects, resulting in a sharp interface region between CO_2 and oil components. Under high injection rates, the flow pathways of CO_2 may increase due to the large injection pressure, making CO_2 easier to break through narrow channels. Especially in 3D porous structures, CO_2 breaks through pore spaces that diffusion struggles to access at high injection rates (Fig. 11b). However, with the same volume of CO_2 injected, the reduced displacement time weakens the diffusion effect at high injection rates.

Pore topology also affects the convective-diffusion between CO_2 and oil. Due to differences in pore size and distribution within pore systems, the oil recovery of the two models is inconsistent (Fig. 9). The mean pore diameters of 2D porous media (models S1 and S2) are comparable (Fig. 2b); however, S1 exhibits stronger heterogeneity, with an entropy value of 0.78. The injected CO_2 primarily flows through preferential channels, limiting the sweep efficiency (Fig. 11a). In contrast, the increased homogeneity of S2 promotes a uniform displacement pattern, leading to enhanced displacement efficiency. For 3D porous media, although S1 exhibits slightly higher heterogeneity than S2, its larger pore sizes contribute to enhanced displacement efficiency (Fig. 11b). Pores with diameters exceeding 15 μm account for 71.62% in S1, whereas the mean pore diameter is only 14.4 μm in S2 (Fig. 2d).

4.4 Quantitative description of CO_2 sweep efficiency

Image processing techniques are applied to the simulation results to extract swept areas and unexploited areas of CO_2 miscible flooding, quantitatively describing the CO_2 sweep efficiency. Firstly, the flow channels are identified and pore spaces are extracted based on the CO_2 mass fraction distribution through image segmentation technology (Fig. 12a).

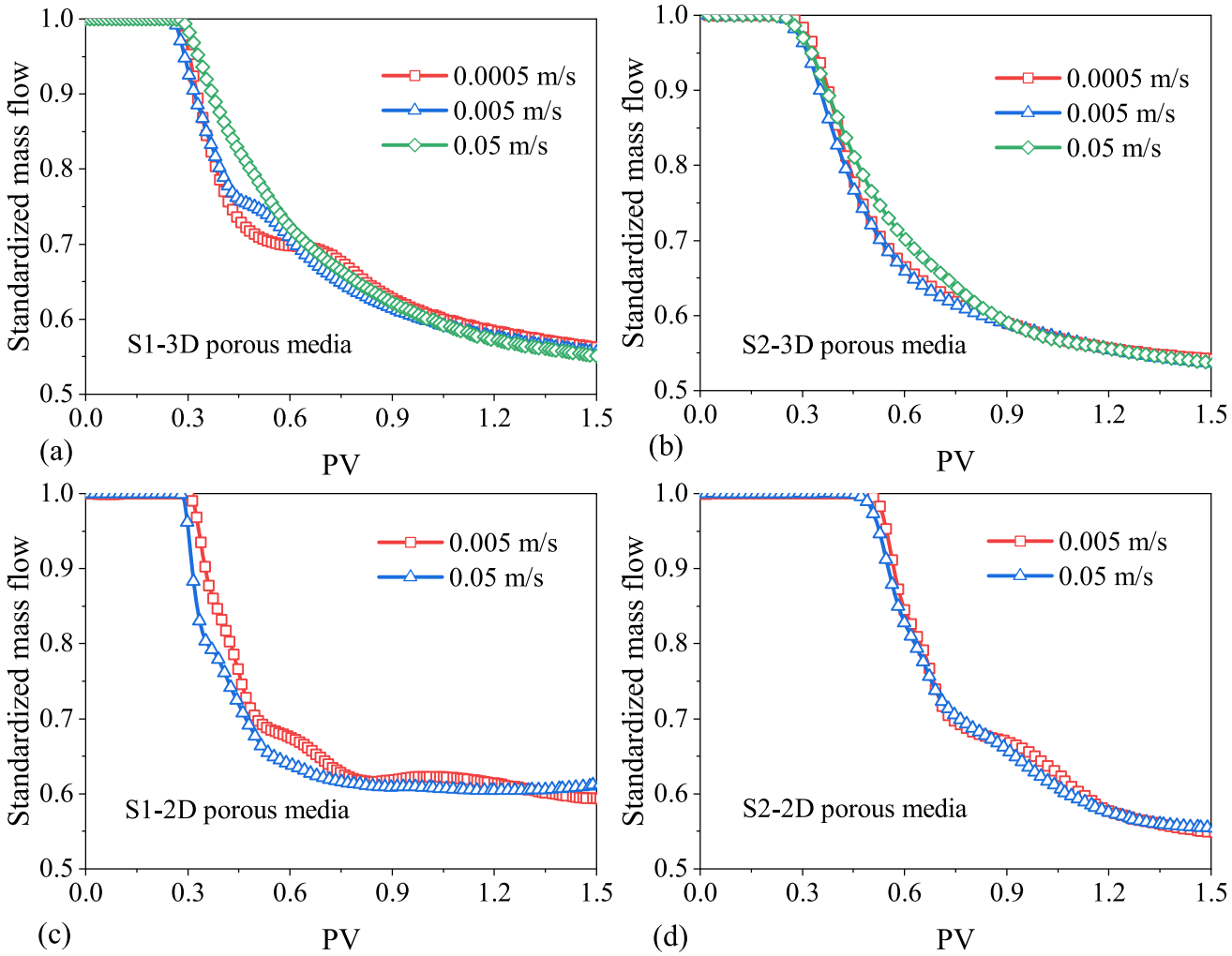

Fig. 10 Effect of CO_2 injection rates on outlet mass flow. **a** S1 and **b** S2 of 3D porous media; **c** S1 and **d** S2 of 2D porous media

To identify the CO_2 sweep area, the RGB images of the CO_2 mass fraction are converted to grayscale images through the blue channel. The grayscale values are negatively correlated with the CO_2 mass fraction, so gray and black regions with varying grayscale values in the images represent the CO_2 sweep areas. Combined with threshold segmentation, the CO_2 sweep areas are marked based on the gray value distribution (Fig. 12b). Then, the distribution of unexploited pores is obtained by subtracting the CO_2 sweep area from the total pore-throat channels using arithmetic expressions. Finally, the watershed algorithm is applied to segment and identify the pore-throat structures (Fig. 12). The segmented pores are distinguished using different colors, enabling a quantitative analysis of the distribution of unexploited pores. For 3D porous media, a circular function is used to automatically extract 100 evenly spaced slices of the CO_2 mass fraction images along the z direction. The CO_2 mass fraction images are also converted into grayscale images with equivalent physical size. In this way, threshold segmentation is performed to obtain 3D CO_2 sweep areas and the distribution characteristics of unexploited pores.

Figure 13 presents the distribution characteristics of unexploited pores, with residual oil in different pores distinguished by various colors in 2D porous media. Due to the convective effect, the oil in the pores near the inlet and within fractures is completely displaced. The bulk CO_2 gradually dissolves into the matrix pores along the fractures due to the diffusion effect. In 2D porous media, low injection rates enhance diffusion effects, leading to widespread CO_2 sweep areas. Conversely, high injection rates result in strong convective effects, making the diffusion of CO_2 into matrix pores along fractures less pronounced, and oil in rough pore surfaces and blind-end pores is not effectively mobilized (Fig. 13). The absence of developed fracture structures in S2 suppresses CO_2 channeling, significantly enhancing the CO_2 sweep efficiency (Fig. 13). In 3D porous media, the displacement efficiency at the injection velocity of 0.005 m/s is the worst. Both decreasing and increasing the injection rates

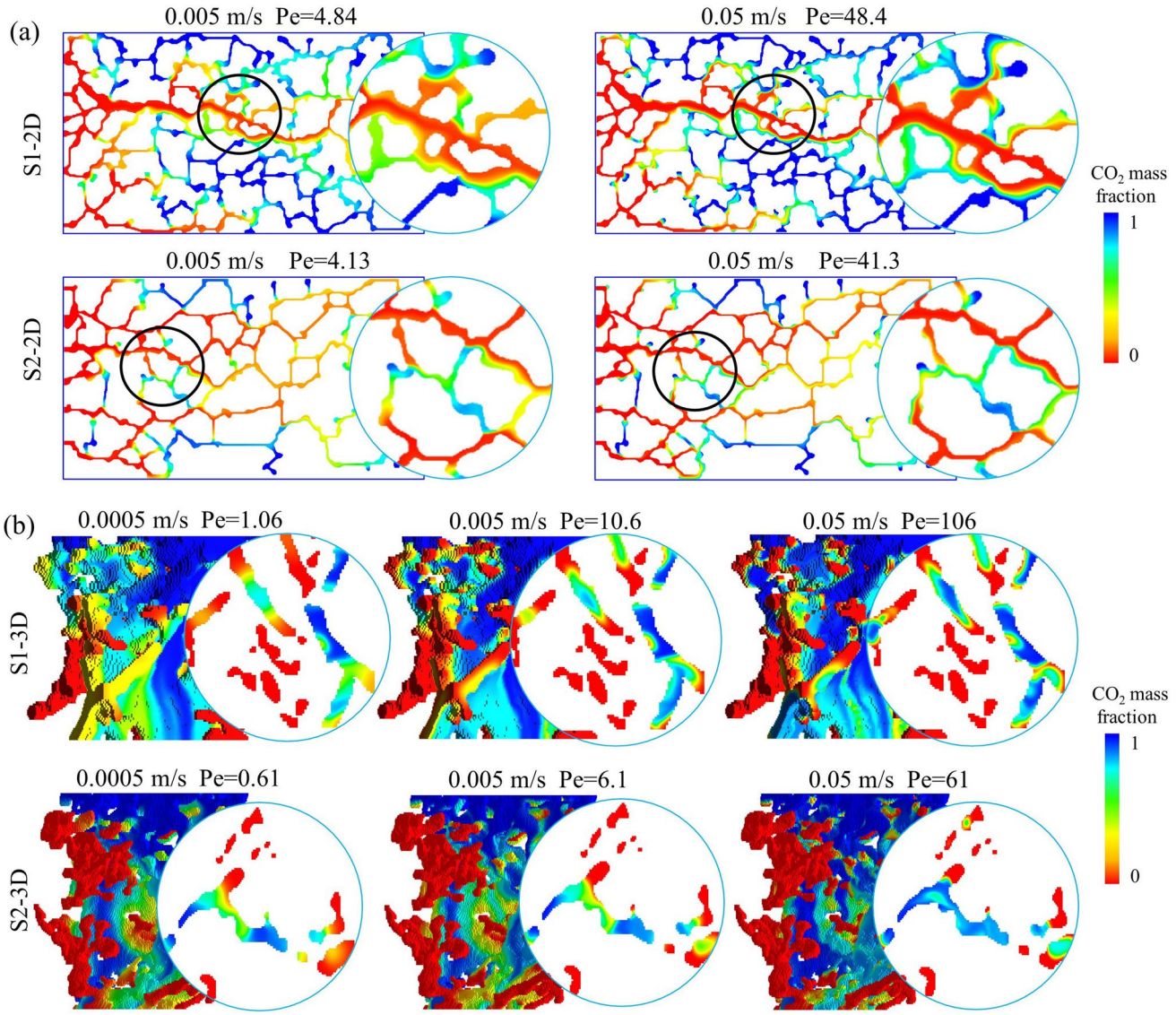

Fig. 11 Distribution of CO_2 mass fraction in **a** 2D and **b** 3D porous media after injecting 1 PV of CO_2

improve the displacement efficiency (Fig. 13c and d). At low flow rates, strong diffusion effectively mobilizes the oil in blind-end pores, while increasing injection rates enhances convection effects, expands the sweep area, and significantly improves recovery.

The distribution characteristics of unexploited pores are obtained under different injection rates (Fig. 14). In 2D porous media of S1, the unexploited pores exhibit an approximately unimodal distribution at low injection rates, with pore diameters mainly concentrated in the range of 6–12 μm, accounting for 66.6% of the total (Fig. 14). In contrast, the unexploited pores display a distinct bimodal distribution at high injection rates, with pore diameters distributed in the ranges of 0–4 μm and 8–14 μm, making up 36.0% and 44.2%, respectively. This indicates that strong diffusion effects significantly mobilize the oil in small pores at low injection rates, but the displacement efficiency is poor in large pore bodies due to the limited diffusion rate. On the contrary, the oil in large pores is effectively displaced due to strong convection effects at high injection rates, but the oil in small pores is less mobilized. Similarly, the unexploited pores exhibit a unimodal distribution at low injection rates in model S2, with 72.1% of unexploited pores distributed in the 6–12 μm diameter range (Fig. 14). At high injection rates, the unexploited pores shift to a bimodal distribution. Due to convection effects, the proportion of unexploited pores in the 6–12 μm diameter range decreases to 48.3%, while the proportion of unexploited pores in the 0–6 μm diameter range increases to 48.4%.

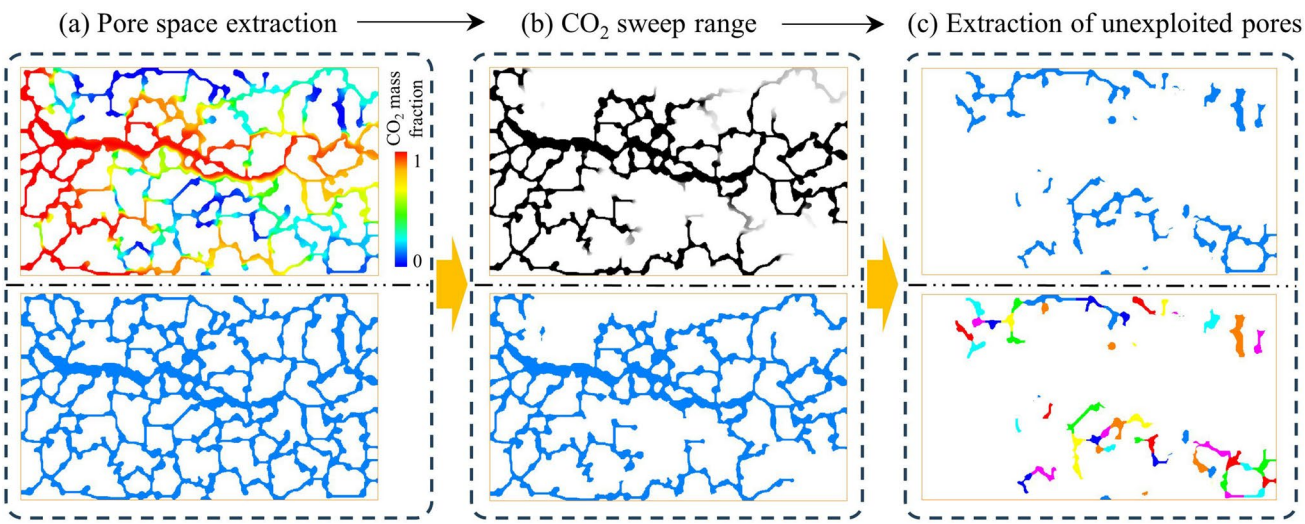

Fig. 12 Quantitative description of the CO_2 sweep efficiency. **a** Extraction of pore-throat channels; **b** Identification of CO_2 sweep areas by image transformation; **c** Analysis of unexploited pores

The effect of injection rate on the distribution of unexploited pores is consistent in 2D and 3D porous media. At high injection rates, oil in large pores is effectively mobilized in 3D porous media, and the diameter of unexploited pores exhibits a distinct unimodal distribution (Fig. 14d). At low injection rates, the proportion of unexploited pores with small diameters significantly decreases. The unexploited pores exhibit a distinct bimodal distribution in model S1, with pore diameters primarily distributed in 0–5 μm and 10–15 μm. Due to the smaller pore size in model S2, the unexploited pores display a unimodal distribution at low injection rates, with the diameter of unexploited pores increasing as the injection rate decreases.

5 Discussion of CO_2 sequestration

5.1 Assessment of CO_2 sequestration capacity

Dissolution and mineralization storage are typically considered to be the permanent CO_2 capture and sequestration mechanisms. During the CO_2 miscible displacement process, a portion of the CO_2 dissolves into the crude oil and is expelled from the outlet, while the remaining CO_2 is trapped within complex pore structures. In pore spaces with higher mobility, CO_2 may be gradually expelled over time. CO_2 trapping primarily results from its dissolution into fluids that become immobilized in inaccessible pore spaces. Therefore, the CO_2 mass fraction within the pore system is insufficient for assessing sequestration capacity. An enhanced evaluation method for carbon sequestration is proposed, which incorporates the velocity distribution. The velocity values within porous structures are normalized, and the sequestration factor (S) is then computed as the ratio of CO_2 mass fraction (φ_{CO_2}) to the normalized velocity:

$$S = \frac{\varphi_{CO_2} \cdot u_{max}}{u} \tag{15}$$

where u_{max} is the maximum velocity and u is the velocity value of the grid node in porous media. A larger sequestration factor indicates a higher CO_2 concentration and reduced fluid mobility in pore spaces, which is favorable for long-term sequestration.

Figure 15 illustrates the CO_2 sequestration characteristics of model S1 at a flow rate of 0.001 m/s. CO_2 concentration is high within fractures, yet the flow exhibits greater mobility, resulting in a weaker sequestration capacity. Additionally, regions with lower CO_2 concentration and slower velocity demonstrate a reduced sequestration potential. However, regions where CO_2 concentration is high but fluid mobility is lower exhibit enhanced sequestration capacity. These areas are typically associated with poor connectivity.

5.2 Effect of injection rate on CO_2 sequestration

The average sequestration factor in porous media is calculated to analyze the impact of injection rate on sequestration (Fig. 16). At the same injection rate, the CO_2 concentration in the porous media rises as the CO_2 injection volume increases, leading to enhanced sequestration capacity. At the early stage of CO_2 injection, the sequestration factor increases slowly, followed by an accelerated growth rate. This suggests that CO_2 primarily occupies high-velocity channels due to convective effects. After breakthrough, CO_2 gradually diffuses into regions favorable for sequestration.

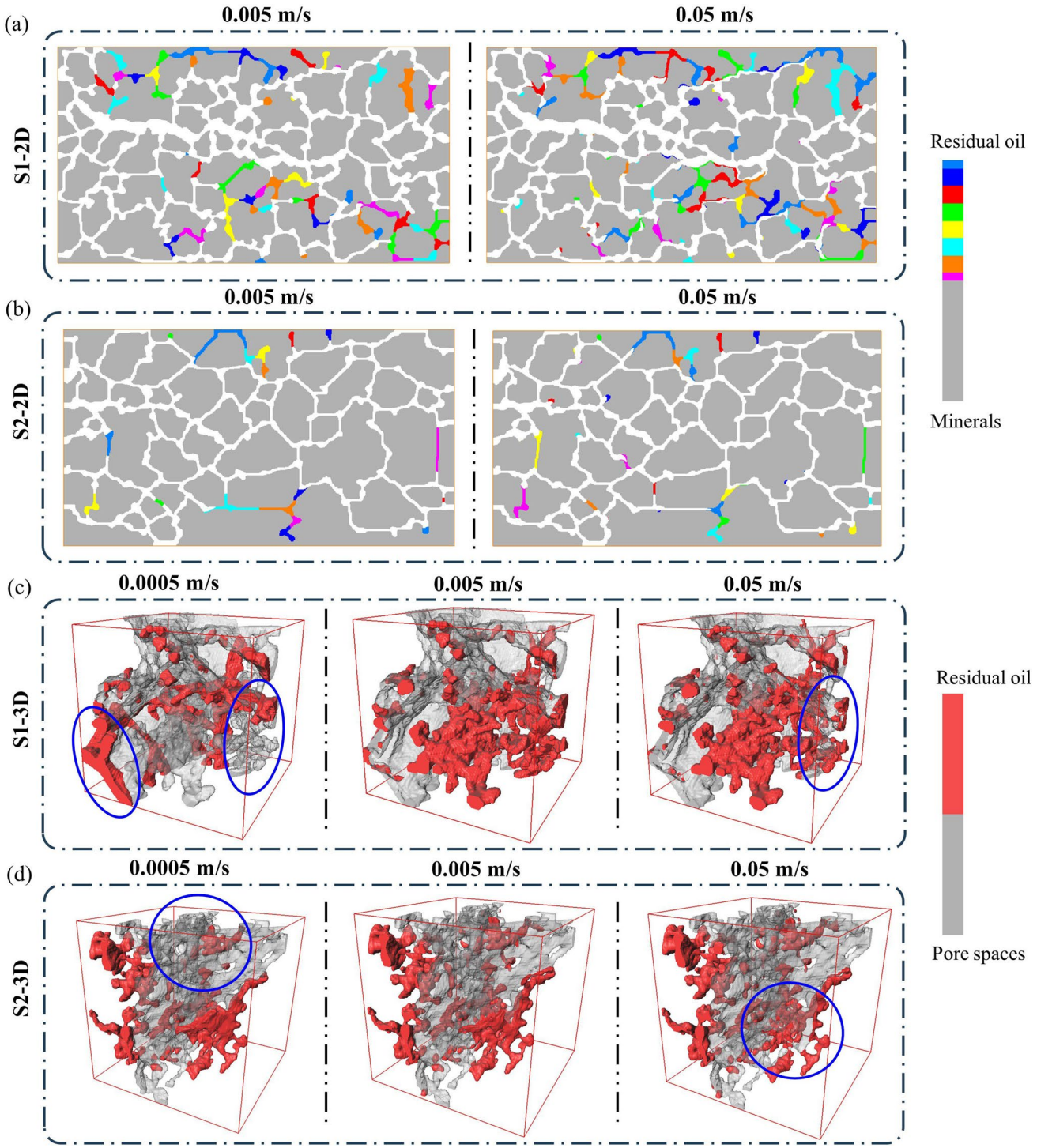

Fig. 13 Distribution characteristics of unexploited pores. Distribution of unexploited pores in 2D porous media of **a** S1 and **b** S2. Distribution of unexploited pores in 3D porous media of **c** S1 and **d** S2

In addition, the sequestration factor exhibits a fluctuating increase in 2D porous media (Fig. 16). This behavior is attributed to the complex pore-throat structures, where CO_2 breaks through multiple flow channels during the displacement process, causing a reduction in sequestration capacity. In contrast, the 3D pore structure model, which is relatively simpler with larger pore throat sizes, shows a steady increase in sequestration capacity as CO_2 is injected (Fig. 16).

The injection rate has a significant impact on sequestration capacity. It is observed that as the injection rate

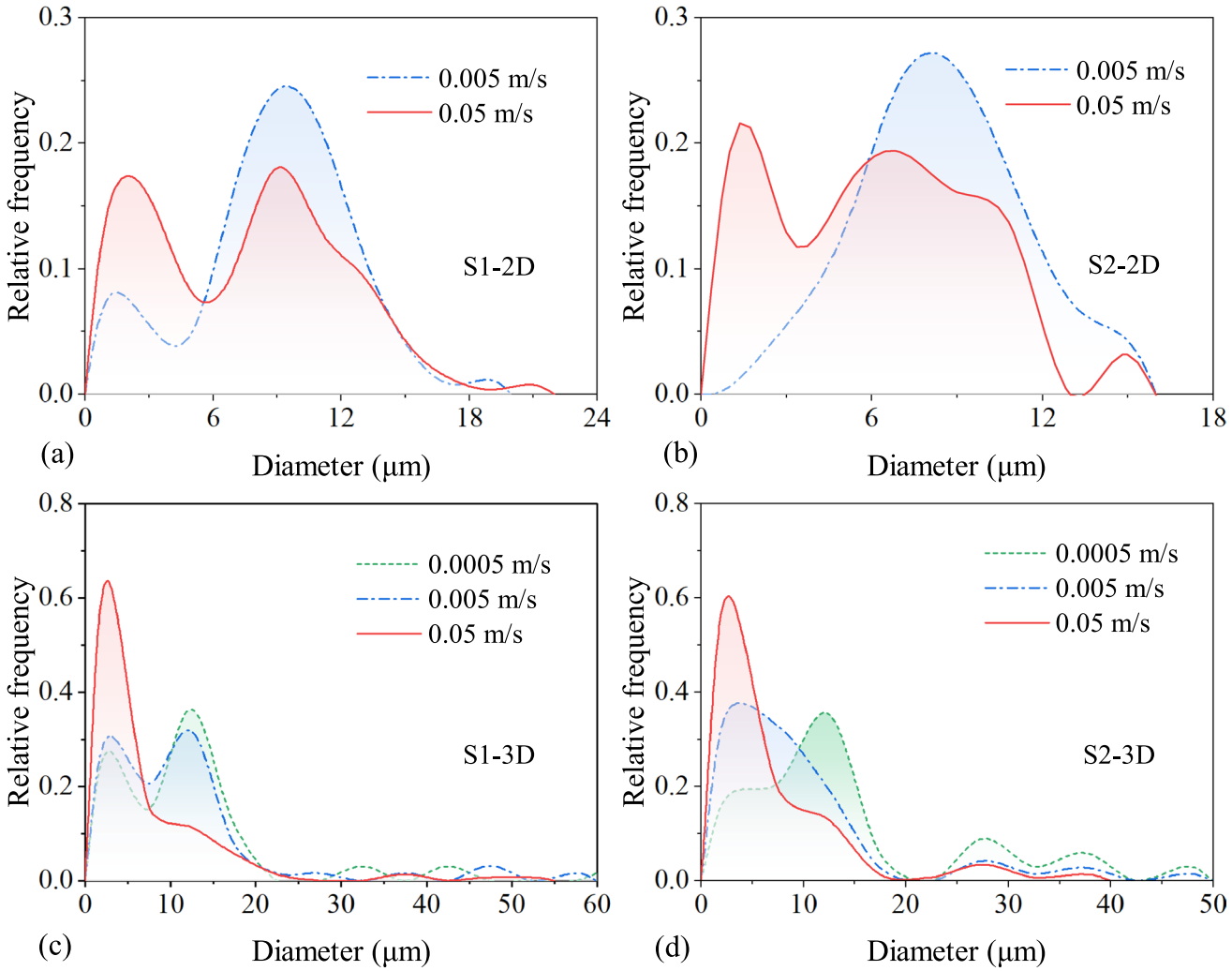

Fig. 14 The relative frequency of unexploited pores as a function of pore diameter. Unexploited pore size distribution of **a** S1 and **b** S2 in 2D porous media, and unexploited pore size distribution of **c** S1 and **d** S2 in 3D porous media

increases, the CO_2 sequestration capacity decreases in 2D and 3D porous media. Although a higher injection rate in the 3D porous media results in an increased CO_2 mass fraction, the rapid flow rate limits the diffusion of CO_2 into the small diameter and blind-end pores within a short period (Fig. 14). These small diameter and poorly connected pores represent favorable regions for CO_2 sequestration. Therefore, a lower injection rate promotes the thorough diffusion of CO_2, enabling it to dissolve and be effectively trapped within these poorly connected pores.

Combining the simulation results, the CO_2 miscible displacement process can be optimized to improve the displacement and storage efficiency. A higher injection rate helps CO_2 occupy large-sized pores and fracture structures, effectively displacing oil in large pore bodies. According to the simulation results of 3D porous media, the convection effect is significant when the injection velocity is greater than 0.005 m/s. To improve oil recovery from heterogeneous and blind-end pores, extended shut-in periods are necessary to enhance the diffusion effects. This facilitates the full dissolution of CO_2, reducing the viscosity and density of the crude oil, and enhancing the sweep efficiency. Additionally, the injected CO_2 is thoroughly dissolved and trapped within the complex pore networks and blind-end pores, improving the sequestration efficiency.

6 Conclusions

This work develops a pore-scale numerical model for CO_2-oil miscible flow. The convection and diffusion mechanisms in complex pore topology are comprehensively analyzed from 2 and 3D perspectives. To optimize CO_2 injection strategies, the CO_2 sweep efficiency and sequestration

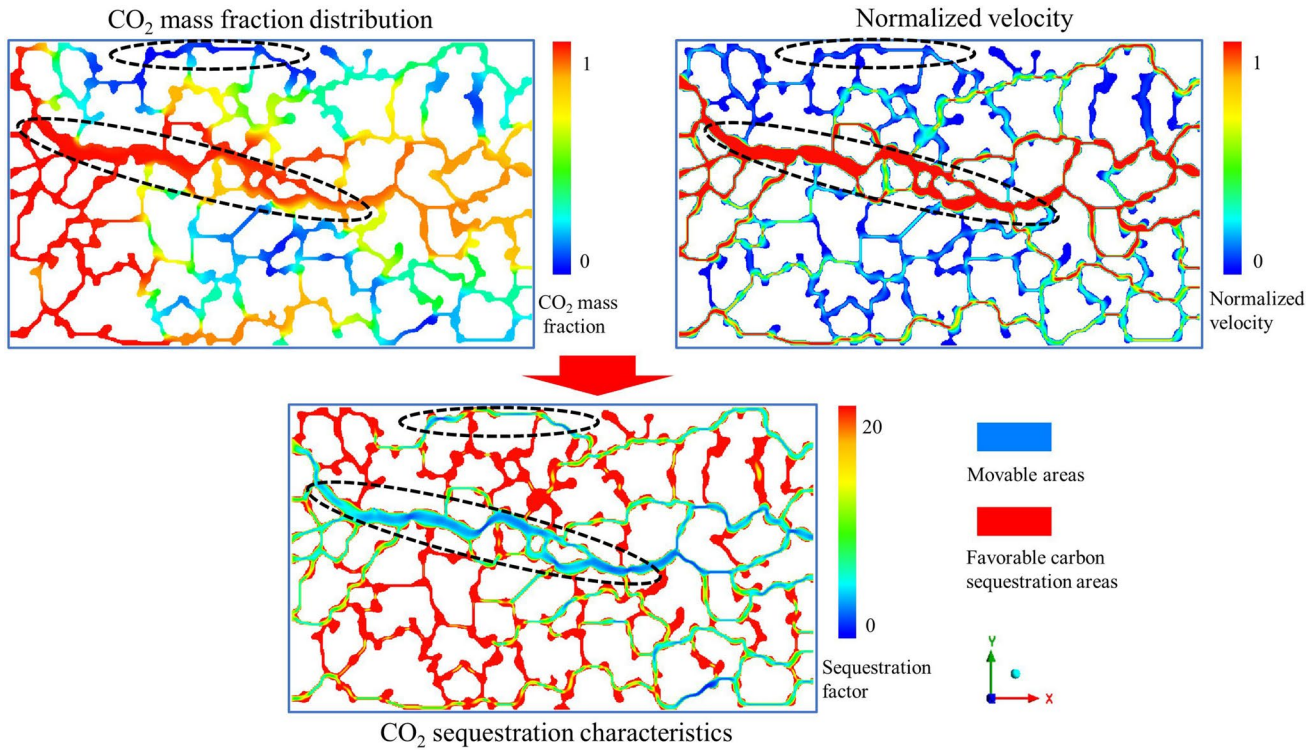

Fig. 15 Evaluation of CO_2 sequestration capacity in complex porous media

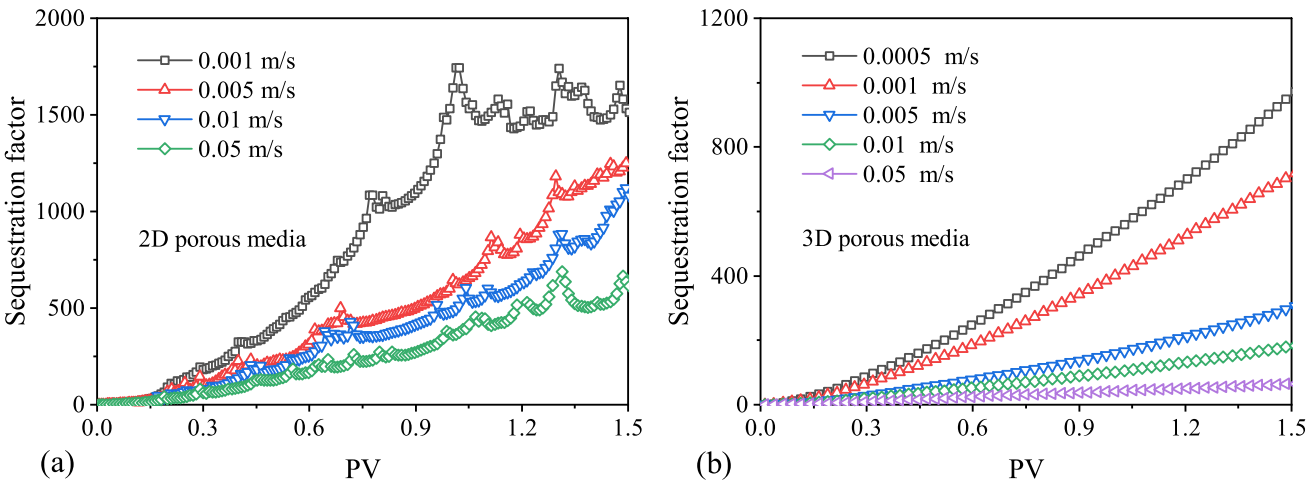

Fig. 16 Sequestration characteristics under different CO_2 injection velocities. **a** 2D porous media; **b** 3D porous media

capacity in complex porous media are evaluated under different injection rates and pore structure properties. The following conclusions are drawn:

(1) Convection dominates displacement before the CO_2 breakthrough, followed by the diffusion of CO_2 from the fractures into the matrix pores. Convection significantly increases the CO_2 mass fraction in fractures with high flow rates, while the CO_2 mass fraction increases slowly in the matrix pores due to diffusion effects. Injected CO_2 reduces fluid pressure, and the injection pressure decreases during CO_2 miscible flooding. The oil recovery increases linearly before the breakthrough, and the increasing rate gradually slows down due to diffusion effects.

(2) The relationship between injection rate and oil recovery differs in 2D and 3D porous media, but the pore mobilization mechanisms are consistent. In 2D porous media,

the injection rate is negatively correlated with oil recovery. In 3D porous media, as the injection rate increases, the oil recovery first decreases and then increases, with the critical velocity being approximately 0.005 m/s. Diffusion effects significantly mobilize oil in small pores at low injection rates, while convection effects predominantly mobilize oil in large pore bodies at high injection rates.

(3) The CO_2 sequestration capacity is evaluated. Diffusion is an important microscopic mechanism for CO_2 sequestration. The injection rate is negatively correlated with the sequestration factor. At low injection rates, CO_2 diffuses into heterogeneous and blind-end pores. The regions with low velocity distribution are favorable areas for CO_2 storage. However, fractures with high velocity are not conducive to long-term storage of CO_2.

Acknowledgements This work was supported by National Natural Science Foundation of China (42172159, 52404048), China Postdoctoral Science Foundation (2023M743870), Postdoctoral Fellowship Program of CPSF (GZB20230864), and Frontier Interdisciplinary Exploration Research Program of China University of Petroleum, Beijing (2462024XKQY002).

Author contributions Xiangjie Qin: Methodology, software, supervision, validation, writing. Han Wang: Methodology, software, supervision. Jinsui Wu: Software, methodology, conceptualization. Gang Wang: Formal analysis, review and editing. David A. Wood: Supervision, validation, writing. Jianchao Cai: Methodology, funding acquisition, review and editing.

Declarations

Conflict of interest The authors declare that they have no known competing financial interests or personal relationships that could have appeared to influence the work reported in this paper.

References

Al-Bayati D, Saeedi A, Myers M et al (2018) An experimental investigation of immiscible-CO_2-flooding efficiency in sandstone reservoirs: influence of permeability heterogeneity. SPE Reservoir Eval Eng 22:990–997

Alfarge D, Wei M, Bai B (2017) Factors affecting CO_2-EOR in shale-oil reservoirs: numerical simulation study and pilot tests. Energy Fuels 31:8462–8480

Alhosani A, Lin Q, Scanziani A et al (2021) Pore-scale characterization of carbon dioxide storage at immiscible and near-miscible conditions in altered-wettability reservoir rocks. Int J Greenhouse Gas Control 105:103232

Bachu S (2016) Identification of oil reservoirs suitable for CO_2-EOR and CO_2 storage (CCUS) using reserves databases, with application to Alberta, Canada. Int J Greenhouse Gas Control 44:152–165

Behnoud P, Khorsand Movaghar MR, Sabooniha E (2023) Numerical analysis of pore-scale CO_2-EOR at near-miscible flow condition to perceive the displacement mechanism. Sci Rep 13:12632

Cai J, Jiao X, Wang H et al (2024a) Multiphase fluid-rock interactions and flow behaviors in shale nanopores: a comprehensive review. Earth-Sci Rev 257:104884

Cai J, Qin X, Xia X et al (2024b) Numerical modeling of multiphase flow in porous media considering micro- and nanoscale effects: a comprehensive review. Gas Sci Eng 131:205441

Chen H, Liu X, Zhang C et al (2022a) Effects of miscible degree and pore scale on seepage characteristics of unconventional reservoirs fluids due to supercritical CO_2 injection. Energy 239:122287

Chen L, He A, Zhao J et al (2022b) Pore-scale modeling of complex transport phenomena in porous media. Prog Energy Combust Sci 88:100968

Chowdhury S, Rakesh M, Medhi S et al (2022) Pore-scale flow simulation of supercritical CO_2 and oil flow for simultaneous CO_2 geo-sequestration and enhanced oil recovery. Environ Sci Pollut Res 29:76003–76025

Du S, Jin J, Shi Y et al (2023) Complex flow in tight oil reservoirs: a new perspective. Mar Pet Geol 150:106095

Edouard MN, Okere CJ, Ejike C et al (2023) Comparative numerical study on the co-optimization of CO_2 storage and utilization in EOR, EGR, and EWR: implications for ccus project development. Appl Energy 347:121448

Franck A, Gisèle F, Thierry Z et al (2024) Comparative study on different coals from the Lorraine basin (France) by sorption isotherms, thermogravimetric analysis and breakthrough curves for CO_2-ECBM recovery. Int J Coal Sci Technol 11(46)

Ge Z, Hou Y, Zhou Z et al (2023) Seepage characteristics of 3D micron pore-fracture in coal and a permeability evolution model based on structural characteristics under CO_2 injection. Nat Resour Res 32:2883–2899

Hao Y, Li Z, Su Y et al (2022) Experimental investigation of CO_2 storage and oil production of different CO_2 injection methods at pore-scale and core-scale. Energy 254:124349

Ho T-HM, Sameoto D, Tsai PA (2021) Multiphase CO_2 dispersions in microfluidics: formation, phases, and mass transfer. Chem Eng Res Des 174:116–126

Iyer G, Ou Y, Edmonds J et al (2022) Ratcheting of climate pledges needed to limit peak global warming. Nat Clim Change 12:1129–1135

Lee C-C, Zhao Y-N (2023) Heterogeneity analysis of factors influencing CO_2 emissions: the role of human capital, urbanization, and FDI. Renewable Sustainable Energy Rev 185:113644

Li S, Li Z, Dong Q (2016) Diffusion coefficients of supercritical CO_2 in oil-saturated cores under low permeability reservoir conditions. J CO_2 Util 14:47–60

Li H-B, Yang Z-M, Li R-S et al (2021) Mechanism of CO_2 enhanced oil recovery in shale reservoirs. Pet Sci 18:1788–1796

Li Z, Liu J, Su Y et al (2023) Influences of diffusion and advection on dynamic oil-CO_2 mixing during CO_2 EOR and storage process: experimental study and numerical modeling at pore-scales. Energy 267:126567

Liu Z, Gao M, Zhang X et al (2023) CCUS and CO_2 injection field application in abroad and china: status and progress. Geoenergy Sci Eng 229:212011

Lu H, Li Q, Yue D et al (2024) Multi-scale pore structure heterogeneity in tuff reservoirs investigated with multi-experimental method and fractal dimensions in chang 7 formation, southern ordos basin. J Earth Sci 35:666–686

Prasad SK, Sangwai JS, Byun H-S (2023) A review of the supercritical CO_2 fluid applications for improved oil and gas production and associated carbon storage. J CO_2 Util 72:102479

Qin X, Xia Y, Qiao J et al (2024) Modeling of multiphase flow in low permeability porous media: effect of wettability and pore structure properties. J Rock Mech Geotech Eng 16:1127–1139

Ramstad T, Berg CF, Thompson K (2019) Pore-scale simulations of single- and two-phase flow in porous media: approaches and applications. Transp Porous Media 130:77–104

Ren J, Xiao W, Pu W et al (2024) Characterization of CO_2 miscible/immiscible flooding in low-permeability sandstones using nmr and the vof simulation method. Energy 297:131211

Seyyedi M, Sohrabi M (2020) Oil reservoir on a chip: Pore-scale study of multiphase flow during near-miscible CO_2 EOR and storage. Transp Porous Media 134:331–349

Shang C, Tang J, Liu W et al (2024) Effects of nanoactive fluids on water wettability reversal of shale: Implications for CO_2 geo-sequestration. Process Saf Environ Prot 190:763–778

Tang Y, Jia C, Chen F et al (2025) Relationship between pore throat structure and crude oil mobility of full particle sequence reservoirs in Permian Fengcheng Formation, Mahu Sag, Junggar Basin, NW China. Pet Explor Dev 52:112–124

Teng L, Li X, Lu S et al (2021) Computational fluid dynamics study of CO_2 dispersion with phase change of water following the release of supercritical CO_2 pipeline. Process Saf Environ Prot 154:315–328

Wan Y, Jia C, Lv W et al (2024) Recovery mechanisms and formation influencing factors of miscible CO_2 huff-n-puff processes in shale oil reservoirs: a systematic review. Adv Geo-Energy Res 11:88–102

Wang H, Su Y, Wang W et al (2022) CO_2-oil diffusion, adsorption and miscible flow in nanoporous media from pore-scale perspectives. Chem Eng J 450:137957

Wang H, Cai J, Su Y et al (2023a) Pore-scale study on shale oil–CO_2–water miscibility, competitive adsorption, and multiphase flow behaviors. Langmuir 39:12226–12234

Wang Y, Shang Q, Guo J et al (2023b) Study on imbibition during the CO_2 enhanced oil recovery in fractured tight sandstone reservoirs. Capillarity 7:47–56

Wang G, Chen X, Liu J et al (2024a) Characterization of coal permeability considering fracture shape—using the mp-otsu threshold segmentation algorithm. J Ind Saf 1:100021

Wang Z, Hu M, Steefel C (2024b) Pore-scale modeling of reactive transport with coupled mineral dissolution and precipitation. Water Resour Res 60:e2023WR036122

Wei B, Gao K, Song T et al (2020) Nuclear-magnetic-resonance monitoring of mass exchange in a low-permeability matrix/fracture model during CO_2 cyclic injection: a mechanistic study. SPE J 25:440–450

Wu Z, Sun Z, Shu K et al (2024) Mechanism of shale oil displacement by CO_2 in nanopores: a molecular dynamics simulation study. Adv Geo-Energy Res 11:141–151

Xu T, Wang J, Lu Y et al (2024) Exploring pore-scale production characteristics of oil shale after CO_2 huff 'n' puff in fractured shale with varied permeability. Int J Coal Sci Technol 11:12

Yang Y, Wang J, Wang J et al (2023) Pore-scale modeling of coupled CO_2 flow and dissolution in 3d porous media for geological carbon storage. Water Resour Res 59:e2023WR035402

Yang L, Liu Y, Wang W et al (2025) Pore-scale flow mechanism of immiscible gas-assisted gravity drainage in strongly heterogeneous glutenite reservoirs. Int J Coal Sci Techn 12:12

Yin Y, Zhang L, Deng H et al (2024) A perspective on fluid dynamics and geochemistry coupling in geologic CO_2 storage: key reactions, reactive transport modeling, and upscaling methods. Gas Sci Eng 130:205421

Yuan L, Zhang Y, Liu S et al (2023) Molecular dynamics simulation of CO_2-oil miscible fluid distribution and flow within nanopores. J Mol Liq 380:121769

Zhang J, Ma G, Yang Z et al (2022) Investigation of flow characteristics of landslide materials through pore space topology and complex network analysis. Water Resour Res 58:e2021WR031735

Zhang X, Xu H, Wang K et al (2023) Integration of domain knowledge and data-driven modeling evaluation process for predicting minimum miscible pressure of CO_2–oil systems in ccus. Energy Fuels 37:18652–18665

Zhu Q, Wu K, Guo S et al (2024) Pore-scale investigation of CO_2-oil miscible flooding in tight reservoir. Appl Energy 368:123439

Zou S, Chen D, Kang N et al (2024) An experimental investigation on the energy signature associated with multiphase flow in porous media displacement regimes. Water Resour Res 60:e2023WR036241